ACCURATE REVERBERATION TIME CONTROL IN FEEDBACK DELAY NETWORKS

Sebastian J. Schlecht and Emanuël A.P. Habets

International Audio Laboratories Erlangen *
Erlangen, Germany
sebastian.schlecht@audiolabs-erlangen.de

ABSTRACT

The reverberation time is one of the most prominent acoustical qualities of a physical room. Therefore, it is crucial that artificial reverberation algorithms match a specified target reverberation time accurately. In feedback delay networks, a popular framework for modeling room acoustics, the reverberation time is determined by combining delay and attenuation filters such that the frequency-dependent attenuation response is proportional to the delay length and by this complying to a global attenuation-per-second. However, only few details are available on the attenuation filter design as the approximation errors of the filter design are often regarded negligible. In this work, we demonstrate that the error of the filter approximation propagates in a non-linear fashion to the resulting reverberation time possibly causing large deviation from the specified target. For the special case of a proportional graphic equalizer, we propose a non-linear least squares solution and demonstrate the improved accuracy with a Monte Carlo simulation.

1. INTRODUCTION

Reverberation time is one of the most prominent acoustical qualities of a physical room dominating the perceptual quality of a space depending on the intended purpose. The reverberation time, denoted by T_{60}, is the most common decay rate measure and is defined as the time needed for the energy decay curve of an impulse response to drop by 60 dB [1]. The frequency-dependent reverberation time $T_{60}(\omega)$ can be similarly derived from the energy decay relief [2]. The accuracy of perceiving the reverberation time has been studied from various application standpoints [3, 4], however, specific just-noticeable-differences may vary depending on the stimulus signal, early to late reverberation ratio and other properties. For a rough orientation, JNDs of 4% have been reported by participants listening to bands of noise [3], 5-12% for impulse responses and 3-9% for speech signals [5].

Consequently, generative algorithms for artificial reverberation strive to recreate the reverberation time of the desired virtual space accurately. Among the algorithms for artificial reverberation, the feedback delay networks (FDNs) enjoy popularity for its versatility and its efficient implementation [6, 7, 8]. The reverberation time of FDNs is commonly determined in two steps: Firstly, a lossless FDN is designed, i.e., the energy entering the FDN cycles unattenuated through the feedback loop such that there is no decay of energy. Secondly, the attenuation filters are introduced in the feedback loop to control the decay rate of the energy and by this the resulting reverberation time of the system. Fig. 1 shows a single feedback comb filter with delay line z^{-m} and attenuation filter $A(z)$.

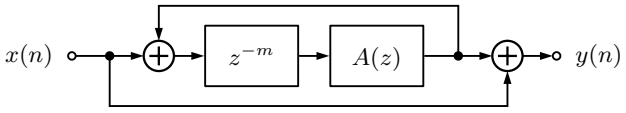

Figure 1: *Feedback comb filter with delay length of m samples and attenuation filter $A(z)$ determining the resulting reverberation time.*

There are commonly two paradigms for designing the attenuation filters: The first being motivated by physical room acoustics, where the reverberation time results from different absorptive boundary materials and the free path in-between [9, 10, 11]. The resulting reverberation time can be predicted by a modified version of Sabine's [12] and Eyering's [13] formulas. Whereas this attenuation filter design is useful for recreating real room acoustics, it is not optimal for achieving precise control of the reverberation time. The second paradigm is motivated from a system theoretic perspective, where attenuation filters influence directly the magnitude of the system poles of the FDN which in turn have a close relation to the resulting reverberation time. The idea is to choose the strength of the attenuation filter proportional to the corresponding delay lengths, i.e., the longer the delay, the stronger is the attenuation [6]. By this, it is possible to define a global *attenuation-per-second* no matter how the signal travels through the delay network.

Various filter types have been proposed to realize the attenuation filter $A(z)$ depending on the control flexibility, computational complexity and required accuracy. In the early days, the most cheaply available filter was a one-pole lowpass filter [6, 14, 15, 16, 17, 18]. Biquadratic filters allow control of the decay time in three independent frequency bands, with adjustable crossover frequencies [19, 20]. More advanced studies try to emulate the frequency response of reflection coefficients in octave bands by applying high-order filter IIR filters [9, 10, 21]. Recently, Jot proposed a proportional graphic equalizer being a simple yet effective method to control an arbitrary number of logarithmic bands [22]. Because of its beneficial design, this graphic equalizer is central to the discussion in this work.

Despite of the large number of proposals on the FDN structure and the attenuation filter, only few details are given on the design of the attenuation filter $A(z)$ assuming that the approximation error made is negligible. However, the example given in Fig. 2 demonstrates that an attenuation filter with a maximum approximation error of a few dB may yield a poor approximation of the resulting reverberation time, in fact it has an infinite T_{60} at 2 kHz. The reason for this inconsistency can be found in the reciprocal relation between the attenuation filter response and the

* The International Audio Laboratories Erlangen are a joint institution of the Friedrich-Alexander-Universität Erlangen-Nürnberg (FAU) and Fraunhofer Institut für Integrierte Schaltungen IIS.

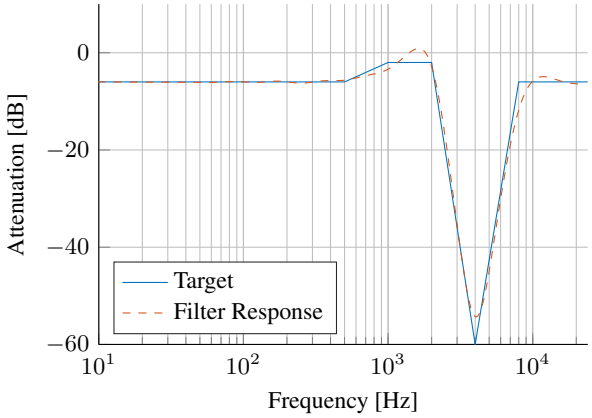

(a) *Target magnitude response of the attenuation filter and an approximated filter.*

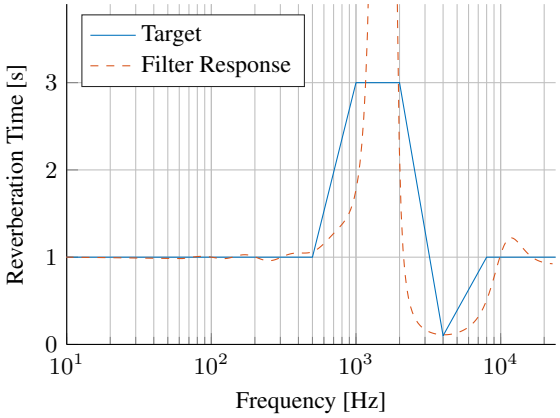

(b) *Corresponding target T_{60} response and the resulting T_{60} of the approximated filter.*

Figure 2: *Target reverberation time and corresponding target attenuation filter magnitude response on the dB scale for a delay m of 100 ms. Although the approximated filter exhibits relatively small attenuation errors, it exhibits large errors for the reverberation time.*

reverberation time. The following paper is dedicated to improving the design of the attenuation filter to achieve a more accurate reverberation time. Section 2 introduces the background on FDNs and the error propagation between the magnitude response and the reverberation time. Further it introduces the proportional graphic equalizer used for the implementation of the attenuation filter. Section 3 introduces different techniques to determine the parameters of the graphic equalizers and demonstrates their impact on a case example. Further, a Monte Carlo simulation with randomized frequency-dependent target reverberation time evaluates the quality of the different parameter estimation methods.

2. REVERBERATION TIME OF AN FDN

2.1. Combination of Comb Filters

An FDN consists of multiple delay lines interconnected by a feedback matrix, which is commonly chosen to be a unilossless matrix[1]. The constituting lossless FDN is adaptable to produce a specified reverberation time by extending every delay line with an attenuation filter [6]. Because of the lossless prototype, each attenuation filter can be considered independently and only dependent on the corresponding delay line. Consequently, the remaining paper only considers single delay line FDNs, which are commonly referred to as absorptive feedback comb filters (see Fig. 1). The transfer function of the absorptive feedback comb filter in Fig. 1 is

$$H(z) = \frac{1}{1 - A(z)z^{-m}}, \tag{1}$$

where $A(z)$ is the transfer function of the attenuation filter and m is the delay length in samples. Every time the signal traverses the feedback loop, it is affected by the attenuation filter such that this recursive effect can be described as an *attenuation-per-time interval*. Particular care should be taken for the design of the attenuation filter $A(z)$ to ensure the stability of (1). The global target *attenuation-per-sample* $\delta(\omega)$ on dB scale can be related to the frequency-dependent reverberation time $T_{60}(\omega)$ by

$$\delta(\omega) = -60\frac{1}{f_\mathrm{s} T_{60}(\omega)}, \tag{2}$$

where f_s is the sampling frequency. On a linear scale, the attenuation-per-sample is given by

$$D(\omega) = 10^{\delta(\omega)/20}. \tag{3}$$

The attenuation filter $A(z)$ is commonly idealized in having zero-phase such that all system poles of (1) lie on the line specified by $|A(\omega)|^{1/m}$ which in turn determines the decay rate of the FDN [6]. Although this cannot be satisfied strictly, in many designs the attenuation filter delay is small compared to the delay m and can be neglected. To achieve the target reverberation time, the attenuation filter is designed such that [6]

$$\begin{gathered} |A(\omega)| \approx D^m(\omega) \\ \text{or} \\ \alpha(\omega) \approx m\delta(\omega), \end{gathered} \tag{4}$$

where

$$\alpha(\omega) = 20\log_{10}|A(\omega)|. \tag{5}$$

In the following section, we explain the error propagation of the filter response as seen in the example given in Fig. 2.

2.2. Error Propagation of Attenuation Filter Approximation

The design of the attenuation filter may be performed by approximating the target magnitude response either on the dB or linear scale in (4) minimizing an appropriate error norm [24]. First, we focus on a least-squares design approach performed on the dB scale as the main objective such that (4) is expressed as [2]

$$\|\alpha - m\delta\|_2^2. \tag{6}$$

[1] In contrast to lossless feedback matrices used for example in [7], unilossless feedback matrices are lossless for all possible delays. For more information, the reader is referred to [23].

[2] The Euclidean norm $\|\cdot\|_2$ of a continuous frequency response F is given by $\|F\|_2 = \left(\int_0^{2\pi} |F(\omega)|^2 \mathrm{d}\omega\right)^{1/2}$ whereas for a $n \times 1$ vector $\boldsymbol{v}$ the Euclidean norm is $\|\boldsymbol{v}\|_2 = \left(\sum_{i=1}^{n} |v_i|^2\right)^{1/2}$.

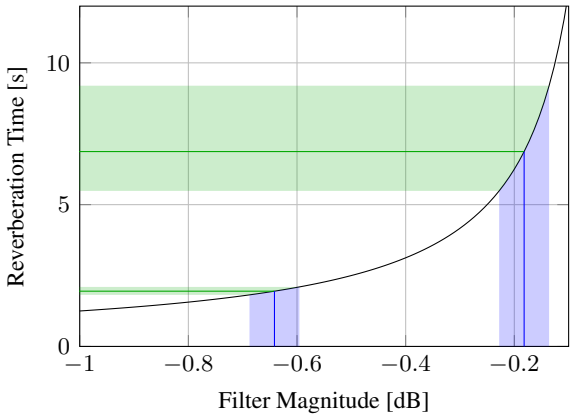

Figure 3: *Error propagation from the filter magnitude response to the resulting reverberation time for a delay m of 100 ms. The black line depicts the relation between filter magnitude and reverberation time as given in* (2) *and* (4)*. The blue shaded intervals indicate error intervals of ± 0.045 dB around two target values (solid blue lines) and the green shaded intervals depict the corresponding error of the reverberation time around the two target values (solid green lines).*

We refer to this approach as the *magnitude least-squares (MLS)* approach.

Because of (2), the approximation error however propagates in a non-linear fashion to the resulting reverberation time. Fig. 3 shows different target magnitudes of an attenuation filter on the dB scale with three equidistant error intervals and corresponding reverberation times. Although the approximation error of the attenuation magnitude is homogenous, the resulting reverberation time can deviate arbitrarily depending on the target value. For strong attenuation of -1 dB, an approximation error of 0.2 dB has neglectable influence on the resulting reverberation time. Whereas for weak attenuation of -0.18 dB the same error can lead to instability as depicted in in Fig. 2.

To overcome this problem, we propose to minimize the error directly on the resulting reverberation time, i.e.,

$$\left\| \frac{1}{\alpha} - \frac{1}{m\delta} \right\|_2^2. \tag{7}$$

We refer to this approach as the T_{60} *least-squares (TLS)* approach. In the following, we discuss the squared errors (6) and (7) for a recently proposed attenuation filter implementation for FDN based on a proportional graphic equalizer [22].

2.3. Proportional Graphic EQ

In the following, we give details on a multiband graphic equalizer allowing logarithmic band adjustment of the reverberation time [22]. The technical details are similar to the ones given in [25, 26]. The graphic multiband equalizer consist of a number of cascaded 2nd order IIR filters, each of which controls a certain band. The lowest and highest band filters are shelving filters [25]:

$$H_{\mathrm{LS},g}(z) = g^{1/2} \frac{p_0 + p_1 z^{-1} + p_2 z^{-2}}{q_0 + q_1 z^{-1} + q_2 z^{-2}} \tag{8}$$

$$H_{\mathrm{HS},g}(z) = g / H_{\mathrm{LS},g}(z) \tag{9}$$

with

$$p_0 = g^{1/2}\Omega^2 + \sqrt{2}\Omega g^{1/4} + 1 \tag{10}$$

$$p_1 = 2g^{1/2}\Omega^2 - 2 \tag{11}$$

$$p_2 = g^{1/2}\Omega^2 - \sqrt{2}\Omega g^{1/4} + 1 \tag{12}$$

$$q_0 = g^{1/2} + \sqrt{2}\Omega g^{1/4} + \Omega^2 \tag{13}$$

$$q_1 = 2g^{1/2}\Omega^2 - 2 \tag{14}$$

$$q_2 = g^{1/2} - \sqrt{2}\Omega g^{1/4} + \Omega^2, \tag{15}$$

where g is the gain at DC ($\omega = 0$) for $H_{\mathrm{LS},g}$ and at the Nyquist frequency ($\omega = f_\mathrm{s}/2$) for $H_{\mathrm{HS},g}$; and $\Omega = \tan(\omega_\mathrm{c}/2)$, where the gain is $g^{1/2}$ at the cutoff frequency ω_c in radians. Whereas the remaining filters are peak-notch filters being defined by the transfer function [25]:

$$H_{\mathrm{PN},g}(z) = \frac{p_0 + p_1 z^{-1} + p_2 z^{-2}}{q_0 + q_1 z^{-1} + q_2 z^{-2}} \tag{16}$$

$$p_0 = g^{1/2} + g\tan(B/2) \tag{17}$$

$$p_1 = -2g^{1/2}\cos(\omega_\mathrm{c}) \tag{18}$$

$$p_2 = g^{1/2} - g\tan(B/2) \tag{19}$$

$$q_0 = g^{1/2} + \tan(B/2) \tag{20}$$

$$q_1 = -2g^{1/2}\cos(\omega_\mathrm{c}) \tag{21}$$

$$q_2 = g^{1/2} + \tan(B/2), \tag{22}$$

where B is the bandwidth which can be alternatively determined by the quality factor Q using $B = \frac{\omega_\mathrm{c}}{Q}$. The cutoff and center frequencies ω_c of the respective band filters are spaced logarithmically over the full frequency range. The so-called *command gain* g of the band filter indicates the maximum boost or attenuation of the magnitude response, respectively.

This parametrization allows that the magnitude responses of the shelving and peak/notch filters at different command gain settings (but with fixed center frequency and bandwidth) are self-similar on the dB scale [27]:

$$g \log_{10} |H_{\mathrm{X},1}| \approx \log_{10} |H_{\mathrm{X},g}|, \tag{23}$$

where $\mathrm{X} \in \{\mathrm{LS}, \mathrm{HS}, \mathrm{PN}\}$ for $H_{\mathrm{X},g}$. Fig. 4a shows the magnitude response of a peak/notch filter for command gains between -30 and 30 dB. It can be observed that the self-similarity property is well-approximated for absolute gains up to 10 dB, but deteriorates for higher absolute gain values. Fig. 4b shows the magnitude response of the individual biquadratic filters of a 9-band graphic equalizer for a prototype gain of 1 dB. There are many refinements for the parametrization of the graphic equalizer, which can be incorporated to further improve the filter design results, e.g. additional opposite filters to reduce the interference between the bands [28], high-precision iterative optimization [29], or improved interpolation of the target response between the center frequencies [30].

The transfer function of the complete graphic equalizer with L-bands is then given by:

$$A_{\mathrm{GE}}(z) = g_0 \prod_{l=1}^{L} H_{l,g_l}(z), \tag{24}$$

where g_0 is an overall broadband gain and H_{l,g_l} is the l^{th}-band with gain g_l, first and last band being low- and high shelving fil-

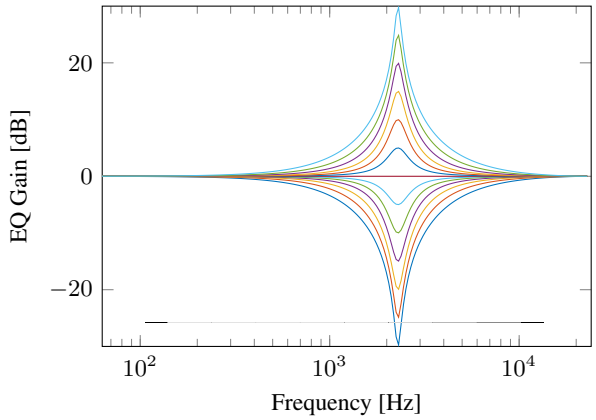

(a) *Single band proportional gain behavior of the magnitude response.*

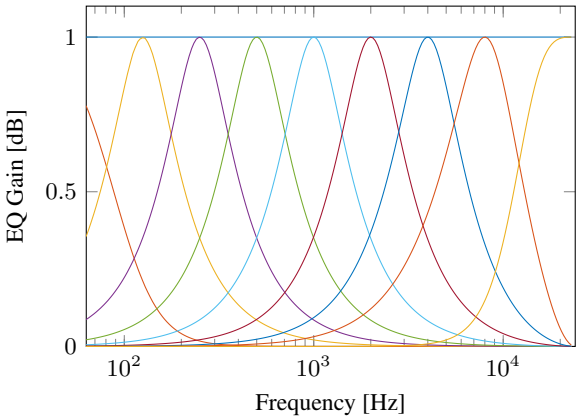

(b) *Prototype magnitude responses for a 9-band graphic equalizer with additional broadband gain as defined in [25].*

Figure 4: *Proportional graphic equalizer as proposed in [22].*

ters and the remaining bands being peak filters. The vector of command gains is then

$$\begin{aligned} \boldsymbol{g} &= [g_0, g_1, \ldots, g_L]^\top \\ \boldsymbol{\gamma} &= 20\log_{10}(\boldsymbol{g}), \end{aligned} \tag{25}$$

where the $\log_{10}$ is applied element-wise, and $(\cdot)^\top$ denotes the transpose operation.

In the next section, we explain the impact of the different error norms on the filter design method for the graphic equalizer and the resulting reverberation time.

3. MULTIBAND GAIN ESTIMATION

3.1. Linear Least-Squares Solution

Because of the self-similarity in (23), the magnitude responses of the band filters can be used as basis functions to approximate the magnitude response of the overall graphic equalizer. The filters are sampled at a $K \times 1$ vector of control frequencies $\boldsymbol{\omega}_\mathrm{P}$ spaced logarithmically over the complete frequency range, where $K \geq L$. The resulting interaction matrix is

$$\begin{aligned} \boldsymbol{B} &= 20\log_{10}\left|[\boldsymbol{g'}, H_{1,g'}(\boldsymbol{\omega}_\mathrm{P}), \ldots, H_{L,g'}(\boldsymbol{\omega}_\mathrm{P})]\right| \\ &= \end{aligned} \tag{26}$$

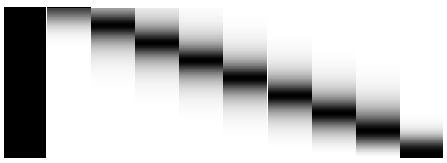

of size $K \times (L+1)$, where g' is a prototype gain and $\boldsymbol{g'} = g'\mathbf{1}_{K\times 1}$. The white color indicates 0 dB gain and dark color indicates gains up to 1 dB in Fig. 4b. The interaction matrix $\boldsymbol{B}$ represents how much the response of each band filter leaks to other bands. Similarly, the target vector is

$$\boldsymbol{\tau} = m\delta(\boldsymbol{\omega}_\mathrm{P}), \tag{27}$$

where δ is applied element-wise. The command gains $\boldsymbol{\gamma}$ for the individual filters yield the resulting magnitude response on the dB scale of the entire attenuation filter:

$$\alpha_\mathrm{GE}(\boldsymbol{\omega}_\mathrm{P}) = \boldsymbol{B}\boldsymbol{\gamma}. \tag{28}$$

The magnitude least squares problem in (6) can then be restated as a linear least-squares problem:

$$\begin{aligned} \boldsymbol{\gamma}_\mathrm{MLS} &= \arg\min_{\boldsymbol{\gamma}} \|\boldsymbol{B}\boldsymbol{\gamma} - \boldsymbol{\tau}\|_2^2 \\ &= (\boldsymbol{B}^\top\boldsymbol{B})^{-1}\boldsymbol{B}^\top\boldsymbol{\tau}, \end{aligned} \tag{29}$$

where $(\boldsymbol{B}^\top\boldsymbol{B})^{-1}\boldsymbol{B}^\top$ is often called the Moore-Penrose pseudoinverse of $\boldsymbol{B}$. The condition number of $\boldsymbol{B}^\top\boldsymbol{B}$ is between 10^5 - $2 \cdot 10^5$, which indicates the inverse operation to be numerically unstable. The pseudoinverse matrix can be computed in advance using the QR-decomposition approach which is numerically more stable than the direct approach, and can then be stored.

3.2. Non-Linear Least-Squares Solution

The T_{60} least-squares problem given in (7) yields then the following nonlinear least-squares problem:

$$\boldsymbol{\gamma}_\mathrm{TLS} = \arg\min_{\boldsymbol{\gamma}} \left\| \frac{1}{\boldsymbol{B}\boldsymbol{\gamma}} - \frac{1}{\boldsymbol{\tau}} \right\|_2^2 = \sum_{k=1}^{K} \left(\frac{1}{(\boldsymbol{B}\boldsymbol{\gamma})_k} - \frac{1}{\tau_k} \right)^2, \tag{30}$$

where $(\boldsymbol{B}\boldsymbol{\gamma})_k = \sum_{l=0}^{L} B_{kl}\gamma_l$. Unfortunately, there is no explicit solution for this non-linear problem such that it has to be solved by a numerical optimization algorithm, e.g., gradient descent algorithm [31]. For gradient based approaches it is efficient and more stable to provide the first and second derivatives analytically. The gradient of (30) is given by

$$\frac{\partial}{\partial\gamma_i} \left\| \frac{1}{\boldsymbol{B}\boldsymbol{\gamma}} - \frac{1}{\boldsymbol{\tau}} \right\|_2^2 = 2\sum_{k=1}^{K} \left(\frac{1}{(\boldsymbol{B}\boldsymbol{\gamma})_k} - \frac{1}{\tau_k} \right) \left(\frac{-B_{ki}}{(\boldsymbol{B}\boldsymbol{\gamma})_k^2} \right)$$

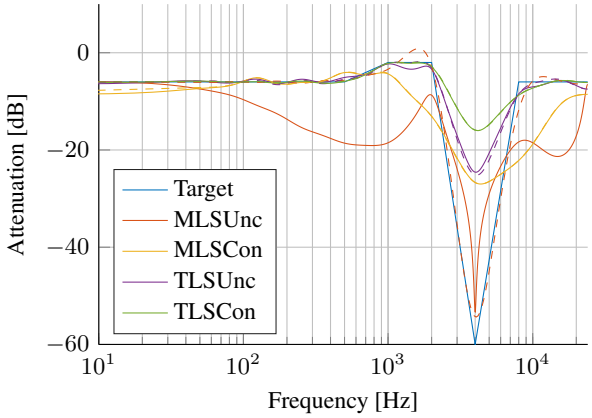

(a) *Magnitude response with different filter design methods.*

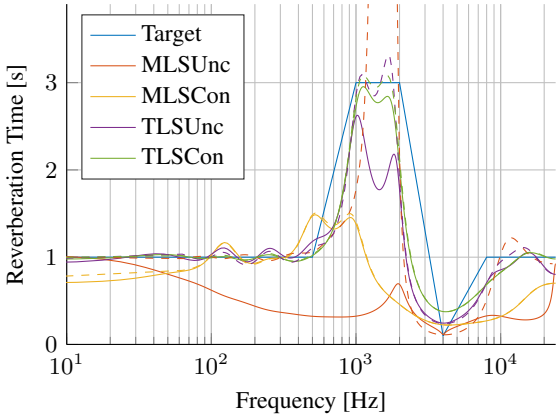

(b) *Reverberation time with different filter design methods.*

Figure 5: *Case study for target reverberation time given in Section 4.1. The dashed lines indicate the approximation response resulting from* (28)*, whereas the solid lines indicate the actual filter response which may differ because of violations of the self-similarity property* (23)*. Both unconstrained methods MLSUnc and TLSUnc has large deviations between the approximation and actual filter response. The TLSCon results in the least error in the resulting reverberation time.*

and the Hessian matrix is given by

$$\frac{\partial^2}{\partial\gamma_i\partial\gamma_j}\left\|\frac{1}{\boldsymbol{B\gamma}}-\frac{1}{\boldsymbol{\tau}}\right\|_2^2 = 2\sum_{k=1}^{K}\frac{B_{ki}B_{kj}}{(\boldsymbol{B\gamma})_k^4}+\left(\frac{1}{(\boldsymbol{B\gamma})_k}-\frac{1}{\tau_k}\right)\left(\frac{2B_{ki}B_{kj}}{(\boldsymbol{B\gamma})_k^3}\right),$$

where $0 \leq i, j \leq L$.

3.3. Constrained LLS and NLLS

Additionally to the least squares problem, we introduce linear constraints on the command gains $\boldsymbol{\gamma}$ to account for the deteriorating self-similarity for large gains in (23):

$$-10 \leq \gamma_l \leq 10 \text{ for } 1 \leq l \leq L, \tag{31}$$

where the value of 10 dB was found empirically. Please note that the first gain γ_0, which is a broadband gain is not limited by a constraint.

In the following, we employ the gradient descent implementation *fmincon* and *fminunc* in MATLAB with and without gain constraints, respectively, to approximate the optimal command gains $\boldsymbol{\gamma}$. For non-linear problems, it is inherent to find a local minimum instead of the globally optimal solution and therefore the choice of the initial value $\boldsymbol{\gamma}^{\text{init}}$ can impact the quality of the solution considerably. Different initial values were tested informally, and for simplicity, we settled for the broadband average gain:

$$\boldsymbol{\gamma}^{\text{init}} = [\overline{\tau}, 0 \ldots, 0], \tag{32}$$

where $\overline{\tau}$ is the arithmetic mean of $\boldsymbol{\tau}$.

4. EVALUATION

Four filter design methods are evaluated in this section:

- MLSUnc: linear unconstrained LS - (29)
- MLSCon: linear constrained LS - (29) & (31)
- TLSUnc: nonlinear unconstrained LS - (30)
- TLSCon: nonlinear constrained LS - (30) & (31)

4.1. Case study

To illustrate some of the shortcomings of a magnitude least squares method for the graphic equalizer, we choose an example target reverberation time and the corresponding target magnitude response values for a delay length of 100 ms. The centre frequencies, the reverberation time definitions and the corresponding target magnitude attenuation are given in Table 1. The large fluctuation in this example was chosen to demonstrate more clearly the potential issues and may be exaggerated in the context of many practical use cases. Table 1 also gives the solutions to the four filter design methods MLSUnc, MLSCon, TLSUnc and TLSCon for a 9-band graphic equalizer and an additional broadband gain. The Fig. 5 shows the resulting attenuation and reverberation time responses for the four methods:

- MLSUnc: The approximation response on the magnitude domain is as expected the best fit to the target magnitude. The corresponding reverberation time deviates strongly, in fact being infinite at 2 kHz. The actual filter response deviates in turn from the approximation in both domains. This is because of a violation of the self-similarity property (23).
- MLSCon: The additional constraints on the command gains $\boldsymbol{\gamma}$ result in a close match between the approximation and the actual filter response. However, the overall filter design quality is poor.
- TLSUnc: The non-linear filter design yields a optimal fit to the target reverberation time, but with a similar deviation from the actual filter response as observed with MLSUnc.
- TLSCon: The additional constraints on the command gains leads to well corresponding approximation and actual filter response and results in a good overall approximation of the target reverberation time response.

Table 1: *Case study corresponding to Fig. 5. The MSE value of the best performing method is indicated in bold.*

Center Frequency ω_c [Hz]		MSE	63	125	250	500	1k	2k	4k	8k	16k
Reverberation Time [s]	T_{60}		1	1	1	1	3	3	0.1	1	1
Magnitude Attenuation [dB]	$\boldsymbol{\tau}$		6	-6	-6	-6	-2	-2	-60	-6	-6
Magnitude errors [dB] at ω_c											
Linear unconstrained LS	MLSUnc	12.08	-1.98	-4.86	-9.31	-12.59	-16.52	-6.72	6.68	-12.35	-15.13
Linear constrained LS	MLSCon	10.28	-1.15	0.85	-0.11	1.92	-2.35	-11.07	33.32	-16.16	-4.30
Nonlinear unconstrained LS	TLSUnc	**9.72**	-0.07	0.55	0.55	0.92	-0.30	-1.38	35.44	-2.48	0.29
Nonlinear constrained LS	TLSCon	12.17	0.08	0.02	0.16	0.11	-0.20	-0.94	44.08	-2.75	0.29
T_{60} errors [s] at ω_c											
Linear unconstrained LS	MLSUnc	0.90	-0.25	-0.45	-0.61	-0.68	-2.68	-2.31	0.01	-0.67	-0.72
Linear constrained LS	MLSCon	0.77	-0.16	0.17	-0.02	0.47	-1.62	-2.54	0.12	-0.73	-0.42
Nonlinear unconstrained LS	TLSUnc	0.42	-0.01	0.10	0.10	0.18	-0.39	-1.22	0.14	-0.29	0.05
Nonlinear constrained LS	TLSCon	**0.32**	0.01	0.00	0.03	0.02	-0.28	-0.96	0.28	-0.31	0.05
Command gain solutions [dB]		γ_0	γ_1	γ_2	γ_3	γ_4	γ_5	γ_6	γ_7	γ_8	γ_9
Linear unconstrained LS	MLSUnc	-0.74	-5.14	-2.84	-3.27	-2.80	-3.48	22.30	-65.06	9.74	-5.76
Linear constrained LS	MLSCon	-18.55	10.00	8.41	5.54	8.13	10.00	5.09	-10.00	-2.36	10.00
Nonlinear unconstrained LS	TLSUnc	-19.77	13.32	7.66	7.89	6.30	9.66	17.64	-18.64	14.05	12.30
Nonlinear constrained LS	TLSCon	-12.15	5.98	3.35	3.76	1.86	6.20	10.00	-10.00	5.02	6.03

To summarize, there are two reasons for poor filter designs: Firstly, the command gains are too large, causing the self-similarity property to deteriorate. The solutions listed in Table 1 also demonstrate that the command gains cannot be simply constraint after the approximation. Secondly, good approximation in the attenuation domain may still result in a poor approximation of the reverberation time. Both shortcomings are overcome by the TLSCon solution resulting in a considerable improvement. In the next section, we expand this result from this specific case study by a Monte Carlo simulation.

4.2. Monte Carlo Simulations

To evaluate the accuracy of the four filter design methods for a large number of target functions, we perform a Monte Carlo simulation. For this, we randomize the target reverberation time T_{60} at nine octave band points with uniform distribution between 0.1 and 5 s. We consider three delay lengths of 10, 100 and 1000 ms. For each condition, we computed 1000 randomized T_{60} responses. The approximation error is quantified by the *mean squared error (MSE)* between the target reverberation time and the approximated reverberation time. Solutions which created an unstable feedback loop were counted separately and are referred to as the *probability of instability*.

Fig. 6 depicts the probability distribution of the MSE for the different filter design methods. The quality of approximation can be observed consistently to the case study in increasing order: MLSUnc, MLSCon, TLSUnc and as the best filter design method TLSCon. The probability of instability is roughly in reversed order with some exceptions. Regarding the three different delay lengths, we can observe:

- $m = 10$ ms: The MSE is relatively small for all four filter design methods. Constrained and unconstrained methods behave largely similar. The MLS methods have a 3-5% chance that the MSE is larger than 2 s, whereas this probability is zero for the TLS methods. The probability of instability is 20% for the MLS methods, whereas it is 0% for TLS methods.
- $m = 100$ ms: Overall, the MSE is slightly larger than for $m = 10$ ms. However, the probability of instability for MLS decreases by up to 7%.
- $m = 1000$ ms: All methods but TLSCon perform considerably worse with the MSE being distributed almost equally up to 2 s. The probability to have an MSE over 2 s is between 15-22% for these methods. The probability of instability for the unconstraint methods is between 19-21%, whereas the constraint methods have a 0% chance to become unstable.

Regarding the impact of the delay length on the MSE, we can observe the following two effects. Firstly, for short delays the target magnitude response is relatively small, e.g., a reverberation time of 5 s corresponds to an attenuation of -0.12 dB per 10 ms, and 0.1 s corresponds to an attenuation of -6 dB per 10 ms. Because of the small target attenuation there is almost no effect from the approximation constraint on the command gains. Further, for MLS methods the target attenuation is close to 0 dB such that the error margin before instability is very narrow causing a high probability of instability. Secondly, long delays deteriorate the approximation quality as the attenuation filter has to attenuate more in one go: a reverberation time of 0.1 s corresponds to an attenuation of -600 dB per 1000 ms, -60 dB per 100 ms and -6 dB per 10 ms. The large attenuation of -600 dB is naturally more difficult to achieve in a controlled fashion than smaller attenuations. The unconstraint methods adapt large command gains causing uncontrolled ripples in the frequency response and therefore unstable feedback. On

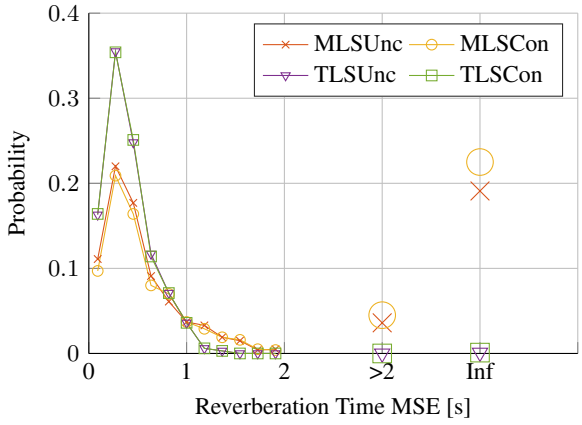

(a) *Monte Carlo simulation with delay length of 10 ms.*

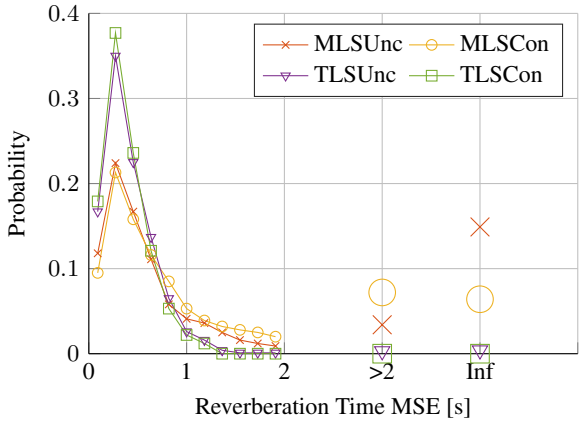

(b) *Monte Carlo simulation with delay length of 100 ms.*

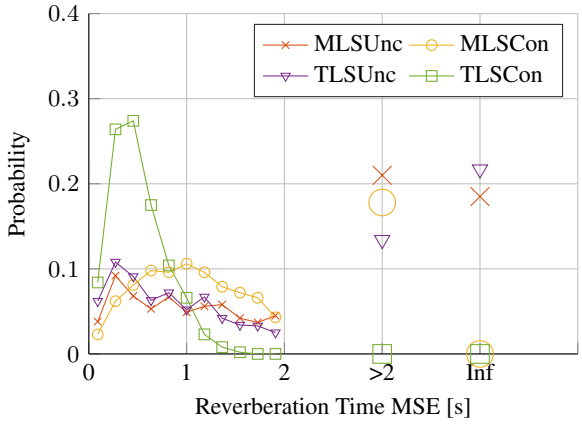

(c) *Monte Carlo simulation with delay length of 1000 ms.*

Figure 6: *Numerical evaluation of the MSE distribution for different filter design methods.*

the contrary, MLSCon chooses a large broadband command gain, and relatively small band command gains such that the filter over-attenuates, which guarantees stable feedback, but causes also large deviation from the target reverberation time. Overall, it can be noted that the proposed filter design method TLSCon outperforms the other methods considerably, especially as it guarantees a stable FDN.

5. CONCLUSION

The impact of different filter design methods of the attenuation filter in an FDN on the resulting reverberation time was investigated. The attenuation filter was implemented by a proportional graphic equalizer. Four methods to compute the parameters were discussed: a linear least-squares problem with and without linear constraint on the command gains approximating the target attenuation magnitude response, and the nonlinear least-squares problem with and without linear constraint approximating the target reverberation time response directly. In a Monte Carlo simulation, we demonstrated that the nonlinear LS solution with linear constraints outperforms the other filter design methods considerably, especially as it guarantees a stable FDN.

This study focus for practicality on a particular filter implementation, however we suggest that it is possible to extend the presented results to other filter types. The proposed approach is difficult to perform in interactive real-time environments such that further investigation in more efficient solutions is required.

References

[1] Manfred R Schroeder, "New Method of Measuring Reverberation Time," *J. Acoust. Soc. Amer.*, vol. 37, no. 3, pp. 409–412, 1965.

[2] Jean Marc Jot, "An analysis/synthesis approach to real-time artificial reverberation," in *Proc. Int. Conf. Acoustics, Speech and Signal Processing*, San Francisco, California, USA, 1992, pp. 221–224.

[3] Hans-Peter Seraphim, "Untersuchungen über die Unterschiedsschwelle exponentiellen Abklingens von Rauschbandimpulsen," *Acta Acustica united with Acustica*, vol. 8, no. 4, pp. 280–284, 1958.

[4] Theodoros I Niaounakis and William J Davies, "Perception of Reverberation Time in Small Listening Rooms," *J. Audio Eng. Soc.*, vol. 50, no. 5, pp. 343–350, 2002.

[5] Matti Karjalainen and Hanna Jarvelainen, "More About This Reverberation Science: Perceptually Good Late Reverberation," in *Proc. Audio Eng. Soc. Conv.*, New York, NY, USA, Nov. 2001, pp. 1–8.

[6] Jean Marc Jot and Antoine Chaigne, "Digital delay networks for designing artificial reverberators," in *Proc. Audio Eng. Soc. Conv.*, Paris, France, Feb. 1991, pp. 1–12.

[7] Davide Rocchesso and Julius O Smith III, "Circulant and elliptic feedback delay networks for artificial reverberation," *IEEE Trans. Speech, Audio Process.*, vol. 5, no. 1, pp. 51–63, 1997.

[8] Vesa Välimäki, Julian D Parker, Lauri Savioja, Julius O Smith III, and Jonathan S Abel, "Fifty Years of Artificial Reverberation," *IEEE Trans. Audio, Speech, Lang. Process.*, vol. 20, no. 5, pp. 1421–1448, July 2012.

[9] Huseyin Hacihabiboglu, Enzo De Sena, and Zoran Cvetkovic, "Frequency-Domain Scattering Delay Networks for Simulating Room Acoustics in Virtual Environments," in *Proc. Int. Conf. Signal-Image Technology Internet-Based Systems*, Dijon, France, 2011, pp. 180–187.

[10] Enzo De Sena, Huseyin Hacihabiboglu, and Zoran Cvetkovic, "Scattering Delay Network: An Interactive Reverberator for Computer Games," in *Proc. Audio Eng. Soc. Conf.*, London, UK, Feb. 2011, pp. 1–11.

[11] Enzo De Sena, Huseyin Hacihabiboglu, Zoran Cvetkovic, and Julius O Smith III, "Efficient Synthesis of Room Acoustics via Scattering Delay Networks," *IEEE Trans. Audio, Speech, Lang. Process.*, vol. 23, no. 9, pp. 1478–1492, 2015.

[12] Wallace Clement Sabine, *Collected papers on acoustics*, Reverberation. Harvard University Press, Cambridge, 1922.

[13] Carl F Eyring, "Reverberation Time in "Dead" Rooms," *J. Acoust. Soc. Amer.*, vol. 1, no. 2A, pp. 168–168, Jan. 1930.

[14] James Anderson Moorer, "About This Reverberation Business," *Comput. Music J.*, vol. 3, no. 2, pp. 13–17, June 1979.

[15] William G Gardner, "A real-time multichannel room simulator," *J. Acoust. Soc. Amer.*, vol. 92, no. 4, pp. 2395, 1992.

[16] Davide Rocchesso, Stefano Baldan, and Stefano Delle Monache, "Reverberation Still In Business: Thickening And Propagating Micro-Textures In Physics-Based Sound Modeling," in *Proc. Int. Conf. Digital Audio Effects*, Trondheim, Norway, Nov. 2015, pp. 1–7.

[17] Riitta Väänänen, Vesa Välimäki, Jyri Huopaniemi, and Matti Karjalainen, "Efficient and Parametric Reverberator for Room Acoustics Modeling," in *Proc. Int. Comput. Music Conf.*, Thessaloniki, Greece, 1997, pp. 200–203.

[18] Jon Dattorro, "Effect Design, Part 1: Reverberator and Other Filters," *J. Audio Eng. Soc.*, vol. 45, no. 9, pp. 660–684, 1997.

[19] Jean Marc Jot, "Efficient models for reverberation and distance rendering in computer music and virtual audio reality," in *Proc. Int. Comput. Music Conf.*, Thessaloniki, Greece, 1997, pp. 1–8.

[20] Thibaut Carpentier, Markus Noisternig, and Olivier Warusfel, "Hybrid Reverberation Processor with Perceptual Control.," in *Proc. Int. Conf. Digital Audio Effects*, Erlangen, Germany, 2014, pp. 93–100.

[21] Torben Wendt, Steven van de Par, and Stephan D Ewert, "A Computationally-Efficient and Perceptually-Plausible Algorithm for Binaural Room Impulse Response Simulation," *J. Audio Eng. Soc.*, vol. 62, no. 11, pp. 748–766, 2014.

[22] Jean Marc Jot, "Proportional Parametric Equalizers - Application to Digital Reverberation and Environmental Audio Processing," in *Proc. Audio Eng. Soc. Conv.*, New York, NY, USA, Oct. 2015, pp. 1–8.

[23] Sebastian J Schlecht and Emanuel A P Habets, "On Lossless Feedback Delay Networks," *IEEE Trans. Signal Process.*, vol. 65, no. 6, pp. 1554–1564, Mar. 2017.

[24] John G Proakis and Dimitris G Manolakis, *Digital Signal Processing*, Upper Saddle River, New Jersey, 4th edition, 2007.

[25] Vesa Välimäki and Joshua Reiss, "All About Audio Equalization: Solutions and Frontiers," *Applied Sciences*, vol. 6, no. 5, pp. 129, May 2016.

[26] Robert Bristow-Johnson, "The Equivalence of Various Methods of Computing Biquad Coefficients for Audio Parametric Equalizers," in *Proc. Audio Eng. Soc. Conv.*, San Francisco, CA, USA, Nov. 1994, pp. 1–10.

[27] Jonathan S Abel and David P Berners, "Filter Design Using Second-Order Peaking and Shelving Sections.," in *Proc. Int. Comput. Music Conf.*, Miami, USA, 2004, pp. 1–4.

[28] Seyed-Ali Azizi, "A New Concept of Interference Compensation for Parametric and Graphic Equalizer Banks," in *Proc. Audio Eng. Soc. Conv.*, Munich, Germany, Apr. 2002, pp. 1–8.

[29] Jussi Rämö, Vesa Välimäki, and Balázs Bank, "High-Precision Parallel Graphic Equalizer," *IEEE Trans. Audio, Speech, Lang. Process.*, vol. 22, no. 12, pp. 1894–1904, Dec. 2014.

[30] Jose A Belloch and Vesa Välimäki, "Efficient target-response interpolation for a graphic equalizer," in *Proc. Int. Conf. Acoustics, Speech and Signal Processing*, Shanghai, China, 2016, pp. 564–568.

[31] Jorge Nocedal and Stephen J Wright, *Numerical Optimization*, Springer Series in Operations Research and Financial Engineering. Springer Science & Business Media, New York, Jan. 1999.